ilmedia

TECHNISCHE UNIVERSITÄT
ILMENAU

Kullig, Julius; Yi, Chang-Hwan; Hentschel, Martina; Wiersig, Jan:

Exceptional points of third-order in a layered optical microdisk cavity

Original published in:	New journal of physics : the open-access journal for physics. - [Bad Honnef] : Dt. Physikalische Ges. - 20 (2018), art. 83016, 10 pp.
Original published:	2018-08-09
ISSN:	1367-2630
DOI:	10.1088/1367-2630/aad594
[*Visited:*	2019-03-27]

This work is licensed under a Creative Commons Attribution 3.0 Unported license. To view a copy of this license, visit http://creativecommons.org/licenses/by/3.0/

TU Ilmenau | Universitätsbibliothek | ilmedia, 2019
http://www.tu-ilmenau.de/ilmedia

New Journal of Physics
The open access journal at the forefront of physics

Deutsche Physikalische Gesellschaft DPG
IOP Institute of Physics

Published in partnership with: Deutsche Physikalische Gesellschaft and the Institute of Physics

OPEN ACCESS

RECEIVED
27 June 2018

ACCEPTED FOR PUBLICATION
24 July 2018

PUBLISHED
9 August 2018

Original content from this work may be used under the terms of the Creative Commons Attribution 3.0 licence.

Any further distribution of this work must maintain attribution to the author(s) and the title of the work, journal citation and DOI.

PAPER

Exceptional points of third-order in a layered optical microdisk cavity

Julius Kullig[1,2], **Chang-Hwan Yi**[1], **Martina Hentschel**[2] **and Jan Wiersig**[1]

[1] Institut für Physik, Otto-von-Guericke-Universität Magdeburg, Postfach 4120, D-39016 Magdeburg, Germany
[2] Institut für Physik, Technische Universität Ilmenau, D-98693 Ilmenau, Germany

E-mail: julius.kullig@ovgu.de

Keywords: microcavity, dielectric cavity, exceptional points, non-Hermitian physics, optical modes

Abstract

A striking signature of the non-Hermitian physics in open systems is the existence of exceptional points (EPs) in parameter space. In contrast to a conventional degeneracy, an EP involves not only the coalescence of the eigenvalues but simultaneously that of the corresponding eigenstates as well. Here, we study EPs in optical microdisk cavities with a concentrically layered refractive index profile. For the double-layered cavity we show the existence of an EP with two coalescing modes. For a triple-layered cavity we verify and discuss the emergence of an EP involving three coalescing modes in a single microdisk cavity.

1. Introduction

Open quantum (or wave) systems are in general described by a non-Hermitian Hamiltonian. An interesting signature of the resulting non-Hermitian physics are exceptional points (EPs) in parameter space where at least two eigenvalues (complex frequencies) and simultaneously also the corresponding eigenstates (modes) coalesce [1–3]. Recently, a lot of theoretical and experimental studies of EPs have emerged in various fields such as $\mathcal{PT}$-symmetric systems [4–6], photonic lattices [7], Bose–Einstein condensates [8], hydrogen atoms [9], microlasers [10], acoustical [11, 12], microwave [13, 14] or optical [15, 16] resonators or photonic crystals [17].

One direct application utilizing the unique properties of EPs are sensors [18–20]. More precisely, the characteristic topology of the eigenvalues around the EP can be used to enhance the sensitivity of such devices. In general the response to an external perturbation at a conventional (diabolic) degeneracy is linear whereas at an EP a characteristic square-root behavior exists. In order to further increase the sensitivity for such sensors EPs of higher order have been considered [21]. In particular, a sensor operating at an EP of third order (EP3) where exactly three eigenstates coalesce has generically a higher sensitivity than a sensor at an EP of second order (EP2) due to the steeper slope of the now cubic root in comparison to a square root under slight perturbations.

For optical microcavities [22, 23] several possibilities to generate EP2s have been devised in the recent years. For example, external scatterers such as nanoparticles or fiber tips can be used to realize an EP2 consisting of purely (counter-)clockwise propagating modes [15, 24, 25]. Furthermore, strong [26] as well as extremely weak [27] boundary deformations are capable to generate EP2s. Yet other possibilities are the adjustment of gain and/or loss [16, 28–30] or the use of absorptive biaxial systems [31].

In comparison to an EP2, however, the preparation of an EP3 is a challenging task but experimentally feasible [12, 21]. In pioneering works usually simple models are considered, e.g., describing the behavior of individually pumped coupled waveguides [4, 32, 33] or cavities [21, 34, 35]. Only quite recently EP3s have been studied as the solutions of full Maxwell's equations for a setup with three coupled waveguides with gain and loss [36].

In this paper, we present a class of microdisk cavities with a layered refractive index structure where both EP2s and EP3s can be realized in a single microcavity geometry. The EPs are achieved without fragile external perturbations and without an additional adjustment of gain and loss. Instead, we use a fine-tuning of the real effective refractive index profile of the cavity, see figure 1 for an example. Moreover, the presented setup provides relatively high Q-factors since the evolved modes are whispering-gallery modes in a rotationally symmetric cavity.

© 2018 The Author(s). Published by IOP Publishing Ltd on behalf of Deutsche Physikalische Gesellschaft

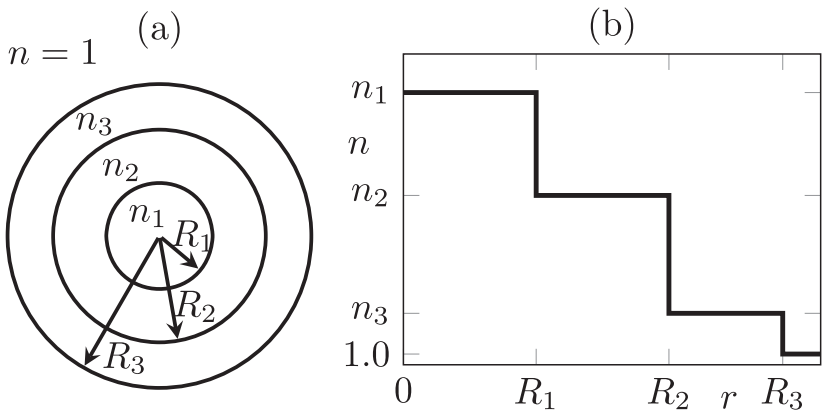

Figure 1. (a) Schematic view of the triple-layered cavity. (b) Refractive index profile for the triple-layered cavity.

The paper is organized as follows. In section 2 we introduce the concentric layered microcavity and explain our scheme to obtain the modes and wave numbers. In section 3 the occurrence of an EP2 in a double-layered cavity is shown and in section 4 the properties of an EP3 in a triple-layered cavity are discussed. The sensing capability of the layered cavity is verified in section 5. A summary with concluding remarks is provided in section 6.

2. The concentric layered cavity

The system studied in this paper is a quasi-two dimensional annular microdisk cavity with N concentric layers of different refractive indexes n_i, $i = 1, \ldots, N$ (see figure 1). Hence, rotational symmetry is preserved. The refractive index n_{N+1} outside of the cavity is assumed to be unity. Moreover, we focus on transverse-magnetic polarization where the electric field is perpendicular to the cavity plane.

In this situation the optical modes, i.e. the solution of Maxwell's equations with harmonic (damped) time dependence, are described by a Helmholtz equation

$$[\nabla^2 + n^2(r)k^2]\Psi(r, \phi) = 0 \tag{1}$$

for Ψ representing the z-component of the electric field. Here, k is the complex wave number which can be redefined to the dimensionless $\Omega = kR$. The real part Re Ω determines the wavelength $\lambda = 2\pi R/\mathrm{Re}\,\Omega$ while the imaginary part Im Ω corresponds to the decay rate $\Gamma = -2\,\mathrm{Im}\,\Omega$ of the mode. Due to the rotational symmetry the angle dependency $\Psi(r, \phi) = \psi(r)\chi_m(\phi)$ with azimuthal mode number m can be separated. If not stated otherwise we will consider the even-parity modes with $\chi_m(\phi) = \cos(m\phi)$; $m = 0, 1, 2, \ldots$. The odd-parity modes can be obtained by replacing $\chi_m(\phi) = \sin(m\phi)$; $m = 1, 2, 3, \ldots$.

In order to solve equation (1) for the layered cavity we make an ansatz for ψ in the ith layer as

$$\psi_i(r) = \mathcal{A}_i J_m(n_i kr) + \mathcal{B}_i H_m(n_i kr), \tag{2}$$

where J_m and H_m are the mth order Bessel and Hankel functions of the first kind. The coefficients $\mathcal{A}_i$, $\mathcal{B}_i$ and the wave number k need to be computed such that (C1) the wave function has no singularity inside the cavity, (C2) at each dielectric interface the boundary conditions

$$\psi_i(R_i) = \psi_{i+1}(R_i), \tag{3a}$$

$$\partial_r\psi_i(R_i) = \partial_r\psi_{i+1}(R_i) \tag{3b}$$

hold, and (C3) Sommerfeld's outgoing wave condition is fulfilled for $r \gg R$.

These conditions lead to the optical modes in the layered microdisk cavity. Note that in [37, 38] a similar problem for circular Bragg reflectors was treated. In distinction, here, the ansatz for ψ is given in terms of Bessel and Hankel functions which is more convenient for the layered dielectric cavity. Hence, our scheme to derive the modes is the following. We enforce (C1) by setting $(\mathcal{A}_1, \mathcal{B}_1) = (1, 0)$. Next, we iterate the coefficient vector via

$$\begin{pmatrix}\mathcal{A}_{i+1}\\ \mathcal{B}_{i+1}\end{pmatrix} = M_i\begin{pmatrix}\mathcal{A}_i\\ \mathcal{B}_i\end{pmatrix} \tag{4}$$

according to the boundary conditions (3) from one layer to the next using the matrices M_i whose matrix elements are

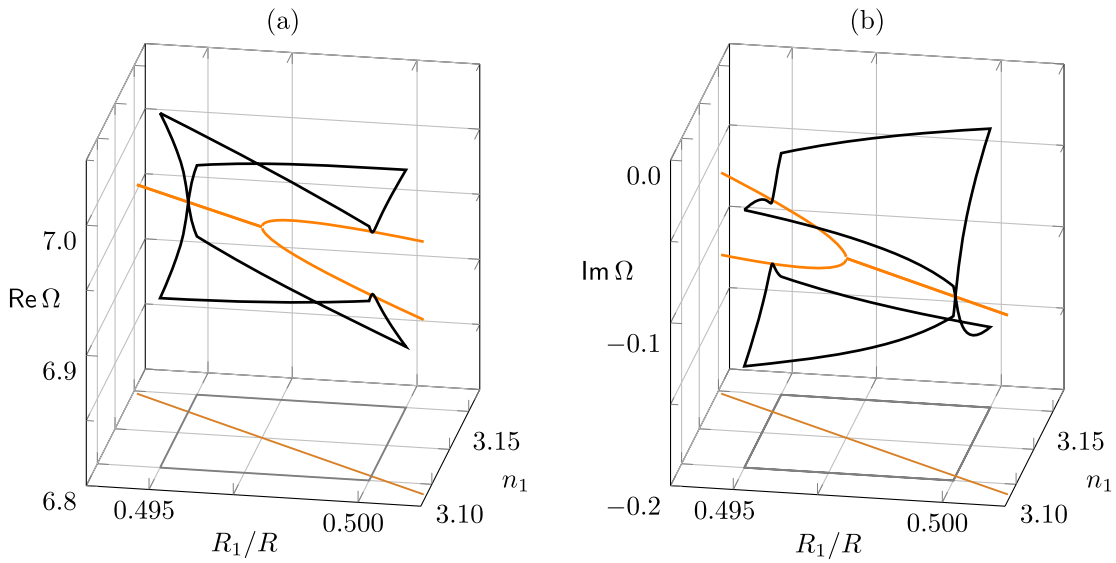

Figure 2. (a) and (b) show the real and the imaginary part of the complex wave number $\Omega = kR$ in a double-layered cavity for two modes with azimuthal mode number $m = 8$. The black curves result from the encircling of the EP2. The orange curve intersecting the EP2 is defined by the parameter configurations where both modes have the same real/imaginary part of Ω. $n_2 = 1.5$ and $R_2 = R$ are fixed.

$$M_{i,11} = \frac{H_m'(n_{i+1}kR_i)J_m(n_ikR_i) - \frac{n_i}{n_{i+1}}J_m'(n_ikR_i)H_m(n_{i+1}kR_i)}{H_m'(n_{i+1}kR_i)J_m(n_{i+1}kR_i) - J_m'(n_{i+1}kR_i)H_m(n_{i+1}kR_i)}, \tag{5a}$$

$$M_{i,12} = \frac{H_m'(n_{i+1}kR_i)H_m(n_ikR_i) - \frac{n_i}{n_{i+1}}H_m'(n_ikR_i)H_m(n_{i+1}kR_i)}{H_m'(n_{i+1}kR_i)J_m(n_{i+1}kR_i) - J_m'(n_{i+1}kR_i)H_m(n_{i+1}kR_i)}, \tag{5b}$$

$$M_{i,21} = \frac{J_m'(n_{i+1}kR_i)J_m(n_ikR_i) - \frac{n_i}{n_{i+1}}J_m'(n_ikR_i)J_m(n_{i+1}kR_i)}{J_m'(n_{i+1}kR_i)H_m(n_{i+1}kR_i) - H_m'(n_{i+1}kR_i)J_m(n_{i+1}kR_i)}, \tag{5c}$$

$$M_{i,22} = \frac{J_m'(n_{i+1}kR_i)H_m(n_ikR_i) - \frac{n_i}{n_{i+1}}H_m'(n_ikR_i)J_m(n_{i+1}kR_i)}{J_m'(n_{i+1}kR_i)H_m(n_{i+1}kR_i) - H_m'(n_{i+1}kR_i)J_m(n_{i+1}kR_i)}. \tag{5d}$$

Here, a prime marks the derivative with respect to the argument. This procedure ensures (C2). Finally, (C3) is enforced via an adjustment of the complex wave number $\Omega = kR$ such that the coefficient $\mathcal{A}_{N+1}$ of the Bessel function in free space vanishes, i.e.

$$\mathcal{A}_{N+1}(\Omega) = 0. \tag{6}$$

The root Ω can be computed numerically, e.g. with Newton's method. Note that the derivative $\mathcal{A}'_{N+1}(\Omega)$ with respect to Ω can be obtained from equation (4) using an iteration scheme as well.

3. EPs of second order (EP2) in a cavity with two layers

The optical (non-concentric) annular cavity has been investigated previously in terms of quantum chaos and dynamical tunneling [39, 40]. On the other hand, in [11] it is reported that a concentric ultrasonic cavity exhibits an EP2 supported by a solid-based mode in the outer layer and fluid-based mode in the inner layer. Hence, the aim of this section is to show that also a concentric optical annular cavity can exhibit a similar EP2 supported by modes in the individual layers. In the parameter configurations we study here the refractive index n_1 of the inner layer is larger than the one of the outer layer. In particular we consider the case where $n_2 = 1.5$ and $R_2 = R$ are fixed but n_1 and R_1 are varied. In figure 2 an EP2 at $(n_{1,\mathrm{EP2}}, R_{1,\mathrm{EP2}}) = (3.1239791, 0.4970147R)$ is shown where Re Ω and Im Ω of two modes with azimuthal mode number $m = 8$ coalesce with $\Omega = 6.961\,85 - 0.089761\mathrm{i}$.

Encircling this EP2 in parameter space by varying n_1 and R_1 (see gray/black curve in figure 2) reveals the characteristic complex square-root topology of Ω in the vicinity of the EP2. In particular, a twofold encircling of the EP2 is needed to restore the initial value of Ω.

Following a particular curve in R_1–n_1 parameter subspace where either Re Ω or Im Ω of the two involved modes are degenerate (see orange curve in figure 2) an intersection with the EP2 can be obtained. This parameter curve is parameterized by $\tau = \mathrm{sign}(\Delta R_1)\sqrt{\Delta R_1^2 + \Delta n_1^2}$ with $\Delta R_1 = (R_1 - R_{1,\mathrm{EP2}})/R$, $\Delta n_1 = n_1 - n_{1,\mathrm{EP2}}$ which measures the Euclidean distance to the EP2. Hence, $\tau < 0$ ($\tau > 0$) refers to parameter combinations of n_1 and R_1

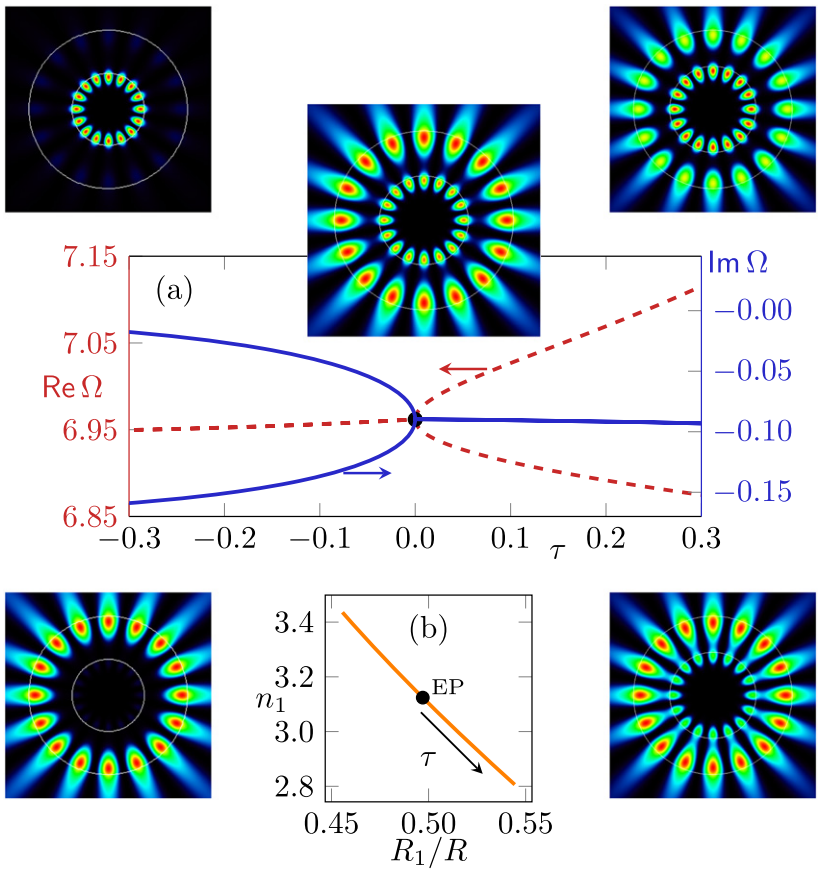

Figure 3. In (a) the (left/red axis/dashed curves) real part and the (right/blue axis/solid curves) imaginary part of the wave numbers $\Omega = kR$ is shown for the two modes with $m = 8$ along the parameter curve plotted as orange curve in (b). The EP2 is marked as a black dot. The intensity mode patterns are shown for $\tau = -0.3, \tau = 0$, and $\tau = 0.3$.

where both involved modes have same Re Ω (Im Ω). Along this parameter curve the modes are analyzed in figure 3. As indicated by the mode patterns a hybrid mode is formed at the EP2 with significant contributions from both the central and the outer layer. As one goes away from the EP2 along the curve of degenerate Re Ω ($\tau < 0$) the system enters the weak coupling regime where individual modes each in either the inner or the outer layer are present.

On the other hand, starting from the EP2 and following the curve of degenerate Im Ω ($\tau > 0$) the system is in the strong coupling regime. Here, two individual non-orthogonal hybrid modes are formed. Hence, the EP2 marks the transition between strong and weak coupling regime of the two layers. Note that in figure 3 the parameter curve is traced over a larger range than in figure 2. It is also mentioned that this parameter curve is not a straight line but slightly curved in the parameter space spanned by n_1 and R_1, see figure 3(b).

4. EPs of third order (EP3) in a cavity with three layers

In this section we consider a triple-layered cavity as illustrated in figure 1. Since the double-layered cavity discussed above exhibits an EP2 formed from modes localized in each layer the natural inference is that a triple-layered cavity is able to exhibit an EP3 as well as EP2s. In this section we confirm the existence of the EP3 in such a cavity.

In order to do so the azimuthal mode number $m = 10$ and the radius $R_3 = R$ are fixed. Hence, the five-dimensional parameter space needed for an EP3 is spanned by R_1, R_2, n_1, n_2, and n_3. In this parameter space we search for configurations where three wave numbers are almost identical, i.e. coalesce, which marks an EP of third order. As a parameter configuration being extremely close to such an EP3 we determine

$$R_{1,\mathrm{EP3}} \approx 0.279906177092R, \tag{7}$$

$$R_{2,\mathrm{EP3}} \approx 0.574914\ 157748R, \tag{8}$$

$$n_{1,\mathrm{EP3}} \approx 5.1445470129, \tag{9}$$

$$n_{2,\mathrm{EP3}} \approx 2.47907903756, \tag{10}$$

$$n_{3,\mathrm{EP3}} \approx 1.38271131243. \tag{11}$$

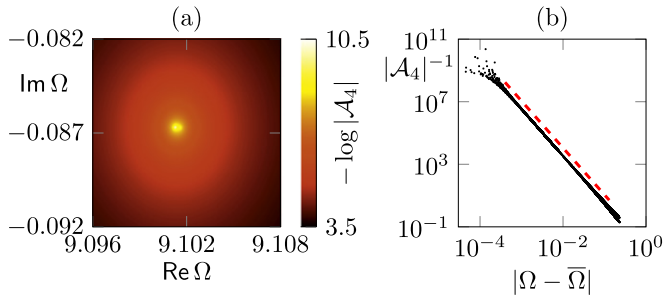

Figure 4. In (a) the modulus $|\mathcal{A}_4(\Omega)|$ (equation (6)) is shown for the optimized configuration (equations (7)–(10)) and $m = 10$ in the complex plane. The color scale is logarithmic. In (b) black dots mark $|\mathcal{A}_4(\Omega)|^{-1}$ which is plotted vs the distance from the mean $\overline{\Omega}$ with double logarithmic axis. The red dashed line indicates the dependency proportional to $|\Omega - \overline{\Omega}|^{-3}$.

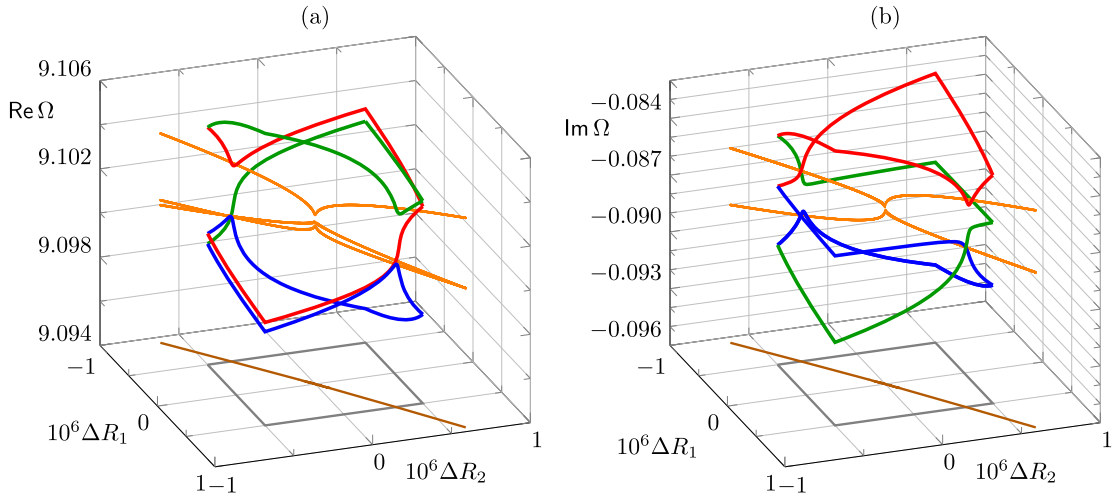

Figure 5. The (a) real and (b) imaginary part of $\Omega = kR$ for modes with $m = 10$ in the three-layered cavity. R_1 and R_2 are varied as $\Delta R_1 = (R_1 - R_{1,\mathrm{EP3}})/R$ and $\Delta R_2 = (R_2 - R_{2,\mathrm{EP3}})/R$. Note that the changes of these parameters are of the order 10^{-6}. The values of Ω for a threefold encircling of the EP3 along the (gray curve) rectangle are shown via the red, blue, and green curves. The orange curves refer to a parameter variation where two modes have (almost) degenerate Im Ω. Note that these curves are partly on top of each other.

However, due to the high sensitivity of the wave numbers around the EP3 and the numerical limits, e.g. in the optimization routine of the configuration or in the solutions of equation (4), we can distinguish even in this optimized configuration three almost degenerate modes as

$$\Omega_1 = 9.101599 - 0.086722\mathrm{i}, \tag{12}$$

$$\Omega_2 = 9.101295 - 0.086697\mathrm{i}, \tag{13}$$

$$\Omega_3 = 9.101252 - 0.086718\mathrm{i}, \tag{14}$$

with mean $\overline{\Omega} = (\Omega_1 + \Omega_2 + \Omega_3)/3$. In spite of these small differences in the following we will verify that the configuration above shows all signatures of an EP3 since it is extremely close to the exact EP3 in parameter space.

First, we verify that the number of almost degenerate modes is exactly three (for each parity class). We analyze $\mathcal{A}_4(\Omega)$ (see equation (6)) for the configuration stated above. In figure 4 it is shown that $|\mathcal{A}_4(\Omega)|$ scales with $|\Omega - \overline{\Omega}|^3$ over several magnitudes. Hence, the configuration is indeed close to a *threefold* root of equation (6). For Ω being very close to $\overline{\Omega}$ the slight differences of $\Omega_1, \Omega_2, \Omega_3$ spoil the correct scaling and for $|\Omega - \overline{\Omega}| > 1$ the scaling is spoiled due to other solutions of equation (6) (not shown in figure 4(b)).

Next, the modes in the very vicinity of the EP3 are analyzed in more detail. Therefore, we restrict ourselves to parameter variations of R_1 and R_2. The other parameters are kept constant as in equations (9)–(11). In this two-dimensional parameter subspace the EP3 is encircled along a rectangular curve. As shown in figure 5 a threefold encircling (red, blue, and green curves for each encircling) is needed to restore the initial value of Ω. This behavior is typical for an EP3. However, it does, strictly speaking, not prove that indeed an EP3 is encircled. As shown in [41] a similar scenario can occur via encircling three times two EP2s.

On the other hand, one can define a curve in parameter subspace of R_1 and R_2 which (almost) intersects the EP3. Here, such a particular curve is constructed by tracing the parameter configurations at which two modes

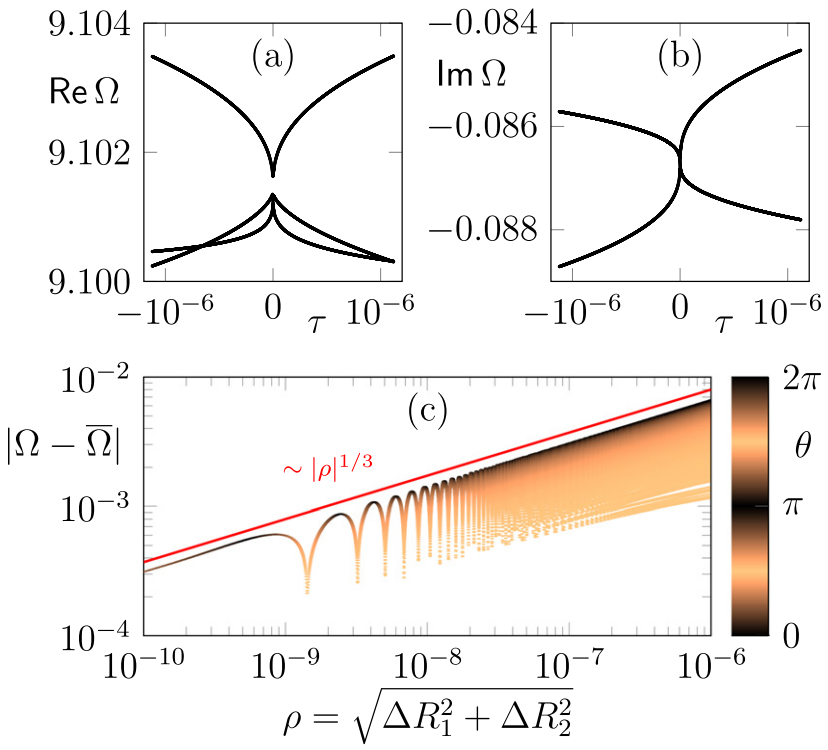

Figure 6. In (a) the real and in (b) the imaginary part of Ω is shown for the three modes with $m = 10$ along the parameter curve (orange curve in figure 5). In (c) dots mark the difference $|\Omega - \overline{\Omega}|$ along a parameter path in R_1–R_2 plane spiraling away from the EP3. The color corresponds to the direction in parameter space as $\theta = [\tan^{-1}(\Delta R_2/\Delta R_1) + \theta_0] \bmod 2\pi$ with $\theta_0 = 0.975$. The red curve indicates the scaling with a cubic root.

have (almost) the same imaginary part of Ω, see orange curve in figure 5. Similar to the previous section this curve is parameterized by $\tau = \text{sign}(\Delta R_1)\sqrt{\Delta R_1^2 + \Delta R_2^2}$ measuring the Euclidean distance to the EP. As indicated in figures 6(a), (b) at $\tau = 0$ the three branches of Ω coalesce marking the EP3.

In order to clearly see the cubic-root behavior of Ω close to the EP3 in figure 6(c) the difference of the wave number Ω to the mean $\overline{\Omega}$ is shown along another parameter curve which starts at the EP and spirals away from it in the R_1–R_2 parameter plane. Hence, along this spiraling parameter curve Ω continuously covers all three Riemann sheets. Simultaneously, by tracing the angle $\theta = [\tan^{-1}(\Delta R_2/\Delta R_1) + \theta_0] \bmod 2\pi$ (color of the dots in figure 6(c)) one uncovers two directions in the parameter space (black dots) where changes in the configuration have the strongest impact on Ω. As expected for an EP3 the difference $|\Omega - \overline{\Omega}|$ indeed scales with a cubic root (red curve). Note that for visibility $\theta_0 = 0.975$ is chosen in figure 6(c). Further note that the wave numbers around an EP3 do not need to follow a cubic-root scaling in every direction in parameter space. As stated in [33] it is possible that in some special directions a square-root scaling is observed.

An additional characteristic of an EP3 is the circling behavior of Ω in the complex plane while the EP3 is encircled three times in parameter space [32, 33, 36]. As already shown in figure 5 (and more clearly in figure 7(d)) we observe this phenomenon via encircling the configuration (7)–(11) in the R_1–R_2 plane along a very small radius $\rho = 10^{-8}R$. For larger radii of the parameter circles the morphology of the Ω-trajectories in the complex plane changes, see figures 7(a)–(c). Such twisted curves are a signature that the parameter loop encloses further EP2s [32, 36]. Nevertheless, the characteristic behavior of the threefold encircling is still visible for the larger parameter loop radii.

Next, the mode pattern at the EP3 is discussed in more detail. First, it is mentioned that the tiny differences between Ω_1, Ω_2, and Ω_3 (see equations (12)–(14)) can be hardly distinguished in the corresponding mode pattern. In particular, their normalized overlap

$$S_{ij} = \frac{\int_0^R \psi_i^*(r)\,\psi_j(r)\,r\mathrm{d}r}{\sqrt{\int_0^R |\psi_i(r)|^2\,r\mathrm{d}r \int_0^R |\psi_j(r)|^2\,r\mathrm{d}r}} \tag{15}$$

has a modulus $|S_{ij}| > 0.999\,999$ close to one. The three modes are therefore highly non-orthogonal as expected. Thus, the mode pattern in figure 8(a) corresponding to Ω_1 is representative for the EP3. It is verified that at the EP3 a hybrid mode is formed with contributions from each layer. The radial intensity plot (figure 8(b)) also

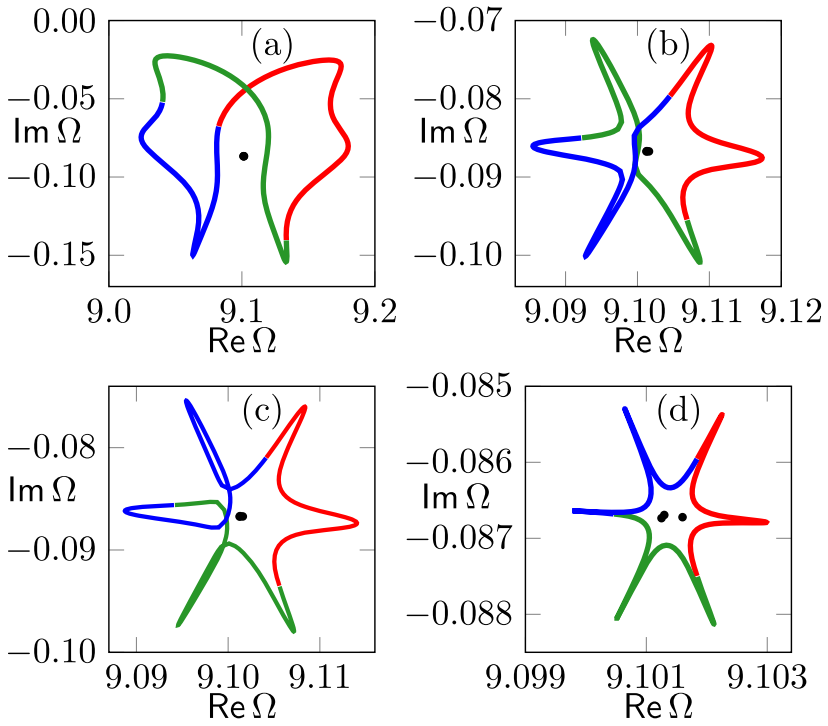

Figure 7. The wave number Ω is traced in the complex plane for a threefold encircling of the EP3 (equations (7)–(11)) in the R_1–R_2 plane. The colors red, green, and blue each corresponds to one encircling. The black dots mark Ω_1, Ω_2, and Ω_3 (equations (12)–(14)). The radii of the circles in the R_1–R_2 plane are (a) $\rho = 10^{-3}R$, (b) $\rho = 10^{-5}R$, (c) $\rho = 5 \times 10^{-6}R$, and (d) $\rho = 10^{-8}R$.

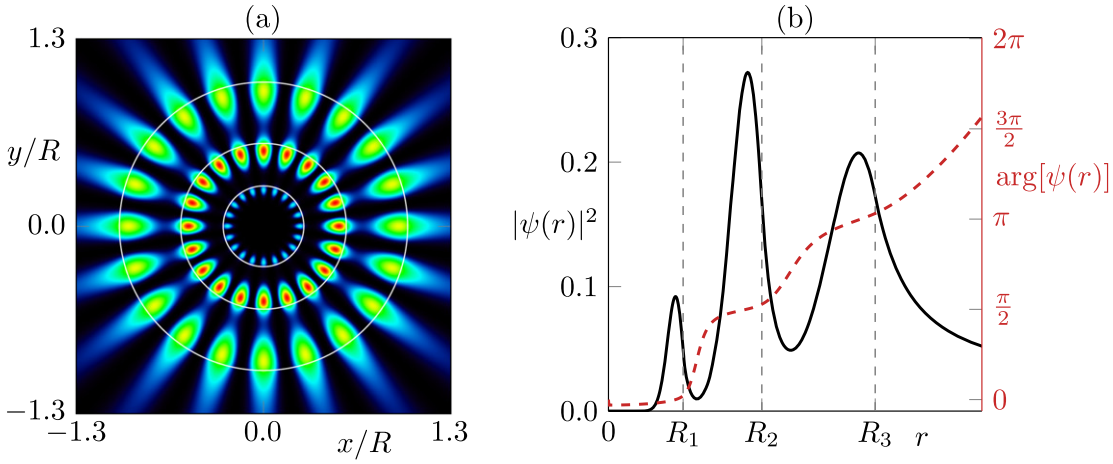

Figure 8. (a) Intensity pattern for the mode $m = 10$ corresponding to Ω_1 (equation (12)) at the EP3. In (b) the (black/left curve/axis) modulus square $|\psi|^2$ as well as the (red/right dashed curve/axis) argument $\arg[\psi(r)]$ of the wave function along $\phi = 0$ are shown.

indicates that the largest contribution comes from the second layer. Moreover, it is mentioned that the phase $\arg[\psi(r)]$ increases stepwise as a function of r inside the cavity, see red curve in figure 8(b). More precisely, the wave function ψ can be projected on a three-component vector S_i representing the normalized contributions from each layer. This can be done by calculating the overlap

$$S_i = \mathcal{N}^{-1} \int_{R_{i-1}}^{R_i} \frac{\psi_i^*(r)}{|\psi_i(R_i)|} \frac{J_m(n_i kr)}{|J_m(n_i kR_i)|} \frac{r\mathrm{d}r}{A_i} \tag{16}$$

with a normalization constant $\mathcal{N}$ such that $\sqrt{|S_1|^2 + |S_2|^2 + |S_3|^2} = 2$, the convention $R_0 = 0$, and the area of the ith layer $A_i = \pi(R_i^2 - R_{i-1}^2)$. In this representation the mode corresponding to Ω_1 is given by

$$\begin{pmatrix} S_1 \\ S_2 \\ S_3 \end{pmatrix} = \begin{pmatrix} 1.1312 \\ 0.0264 + 1.2780\mathrm{i} \\ -1.030 + 0.1586\mathrm{i} \end{pmatrix}. \tag{17}$$

This vector can be interpreted by a simple toy model given by the (dimensionless) non-Hermitian Hamiltonian

$$H = \begin{pmatrix} E - 2\mathrm{i} & \sqrt{2} & 0 \\ \sqrt{2} & E & \sqrt{2} \\ 0 & \sqrt{2} & E + 2\mathrm{i} \end{pmatrix}. \tag{18}$$

Formally, a similar Hamiltonian has been used in [32, 33, 42] for the description of three coupled waveguides with loss and gain. Here, for the triple-layered cavity, the interpretation is the following. The diagonal terms E correspond to the unperturbed eigenvalue of the non-coupled layers. The $\sqrt{2}$ terms are the direct coupling of two adjacent layers. Moreover, an indirect coupling is conveyed by the terms 2i which reflect a better/worse confinement of the modes in the outer/inner layer due to their coupling to the second layer.

The Hamiltonian in equation (18) has an EP3 with a corresponding eigenvector

$$\Psi_{\mathrm{EP}} = \begin{pmatrix} 1 \\ \sqrt{2}\mathrm{i} \\ -1 \end{pmatrix}. \tag{19}$$

This eigenvector nicely reflects the properties of the wave function ψ as it (i) resembles the phases of the entries (see equation (17)) and (ii) explains the dominant contribution in the second layer (see figure 8).

5. Verification of sensing capability

So far we have illustrated the appearance of an EP2 (EP3) in a double- (triple-)layered cavity. The aim of this section is to illustrate the corresponding sensing capability of the cavities. In particular the improved sensitivity at the EP3 is emphasized.

In general several external perturbations could be considered for detection, e.g. external nanoparticles or fiber tips or boundary deformations. However, within the scope of this paper, i.e. a concentric layered cavity, an external perturbation can be realized effectively namely by introducing an additional thin layer at the surface of the cavity. Experimentally such a thin layer can be realized via coating or adhesions at a functionalized cavity boundary where molecules can attach [43–45]. Hence, a high sensitivity is related to a considerable spectral frequency shift, frequency splitting and/or linewidth broadening [19, 46–50] already for a very thin additional layer. In the following we quantify the changes in the frequencies via a relative splitting $\Delta_\omega(d)$ in the real part of Ω and a relative broadening $\Delta_\Gamma(d)$ due to the imaginary part of Ω as function of the thickness d of the additional layer as

$$\Delta_\omega(d) = \frac{\max_i\{\mathrm{Re}[\Omega_i(d)]\} - \min_i\{\mathrm{Re}[\Omega_i(d)]\}}{\max_i\{\mathrm{Re}[\Omega_i(d)]\} + \min_i\{\mathrm{Re}[\Omega_i(d)]\}}, \tag{20}$$

$$\Delta_\Gamma(d) = \frac{\max_i\{|\mathrm{Im}[\Omega_i(d) - \Omega_i(0)]|\}}{\max_i\{|\mathrm{Im}\,\Omega_i(0)|\}}. \tag{21}$$

The index i labeling the modes is $i = 1, 2$ for the double-layered cavity and $i = 1, 2, 3$ for the triple-layered cavity. In the following the refractive index of the additional layer is fixed to $n = 3$. As shown in figure 9 both $\Delta_\omega(d)$ and $\Delta_\Gamma(d)$ show the expected scaling corresponding to the order of the EPs. In particular a cubic-root scaling is verified for the EP3 in the triple-layered cavity (equations (7)–(11)), whereas for the EP2 in the double-layered cavity (figure 3) a square-root scaling is observed. Hence, a sensor based on the EP3 is indeed more sensitive in the detection of very thin additional layers than a sensor operating at an EP2 or a conventional diabolic degeneracy.

6. Summary and concluding remarks

In our paper we introduced the multi-layered optical microdisk cavity with a stepwise refractive index profile. By tuning the parameters of the cavity such as the refractive indexes and the size of the individual layers EPs can be generated. In a double-layered cavity an EP of second order is found with the characteristic square-root topology of the wave numbers in parameter space. In case of a triple-layered cavity we presented a configuration supporting an EP of third order which generates the characteristic triple-root topology of the complex wave numbers.

In the following we list some key remarks and conclusions. (i) The supported modes of the layered cavity are whispering-gallery modes due to the rotational symmetry. They do not suffer Q-spoiling due to boundary

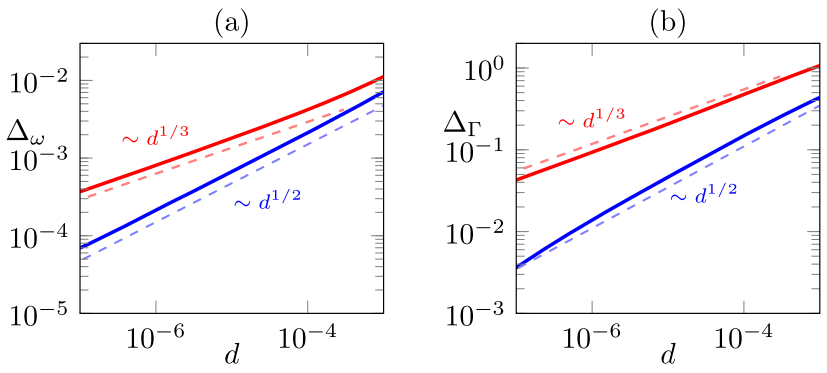

Figure 9. In (a) the relative splitting $\Delta_\omega(d)$ (equation (20)) and in (b) the relative broadening $\Delta_\Gamma(d)$ (equation (21)) is shown as function of the thickness d of an additional layer with refractive index $n = 3$. Solid curves are the numerically obtained values for a (red) triple-layered cavity at the EP3 and a (blue) double-layered cavity at an EP2. Dashed curves illustrate the scaling corresponding to a square root and cubic root.

deformations or external scatterers. (ii) Once the desired configuration of the cavity is fabricated it can be operated quite stable since no external components like nanofiber tips need to be adjusted as in other schemes that have been studied. (iii) Even- and odd-parity modes are double-degenerate for rotational symmetric cavities. Hence, also the achieved EPs are double-degenerate, i.e., one single configuration of the cavity provides an EP for the even- as well as for the odd-parity modes. This is advantageous because it guarantees the same sensitivity of a potential particle sensor along the whole sidewall. (iv) In order to achieve even higher-order EPs, in principle, the number of layers can be stacked. (v) Since even- and odd-parity modes are in fact decoupled in the layered microcavity, in principle, a perturbation in terms of external scatterers or boundary deformations is feasible to couple them. This implies the possibility to generate EPs whose order is twice the number of layers. (vi) An advantage of the proposed layered geometry in comparison to already existing simply connected geometries for EPs is that the mode spreads over all respective layers and therefore has a large mode volume in the cavity. This can be advantageous for the detection of particles not only at the sidewalls but also on top of the microdisk where sensors based on ordinary whispering-gallery modes are typically less sensitive. (vii) An experimental realization of a concentric layered cavity could be the one in [51] where it has already been demonstrated that different materials can be combined to fabricate concentric Bragg reflectors epitaxially around single free standing nanopillars, e.g. for GaAs based nanopillar resonators SiO_x and amorphous Si has been used. In an experiment, however, the proposed values of the configuration need to be slightly adapted respecting the particular conditions in the laboratory. Here a fine tuning of the temperature [52], the environmental gas [45] or a pump power control [53] might be helpful to adjust the EP.

Acknowledgments

Financial support from Emmy Noether Programme of the German Research Foundation (HE-3494/3) is acknowledged.

References

[1] Heiss W D 2012 *J. Phys. A: Math. Theor.* **45** 444016
[2] Kato T 1966 *Perturbation Theory for Linear Operators* (New York: Springer) (https://doi.org/10.1007%2F978-3-662-12678-3)
[3] Berry M 2004 *Czech. J. Phys.* **54** 1039–47
[4] Teimourpour M H, El-Ganainy R, Eisfeld A, Szameit A and Christodoulides D N 2014 *Phys. Rev.* A **90** 053817
[5] Rüter C E, Makris K G, El-Ganainy R, Christodoulides D N, Segev M and Kip D 2010 *Nat. Phys.* **6** 192
[6] Shi C, Dubois M, Chen Y, Cheng L, Ramezani H, Wang Y and Zhang X 2016 *Nat. Commun.* **7** 11110
[7] Regensburger A, Bersch C, Miri M A, Onishchukov G, Christodoulides D N and Peschel U 2012 *Nature* **488** 167
[8] Gutöhrlein R, Main J, Cartarius H and Wunner G 2013 *J. Phys. A: Math. Theor.* **46** 305001
[9] Cartarius H, Main J and Wunner G 2007 *Phys. Rev. Lett.* **99** 173003
[10] Liertzer M, Ge L, Cerjan A, Stone A D, Türeci H E and Rotter S 2012 *Phys. Rev. Lett.* **108** 173901
[11] Shin Y, Kwak H, Moon S, Lee S B, Yang J and An K 2016 *Sci. Rep.* **6** 38826
[12] Ding K, Ma G, Xiao M, Zhang Z Q and Chan C T 2016 *Phys. Rev.* X **6** 021007
[13] Dembowski C, Gräf H D, Harney H L, Heine A, Heiss W D, Rehfeld H and Richter A 2001 *Phys. Rev. Lett.* **86** 787–90
[14] Doppler J, Mailybaev A A, Böhm J, Kuhl U, Girschik A, Libisch F, Milburn T J, Rabl P, Moiseyev N and Rotter S 2016 *Nature* **537** 76
[15] Peng B, Özdemir Ş K, Liertzer M, Chen W, Kramer J, Yılmaz H, Wiersig J, Rotter S and Yang L 2016 *Proc. Natl Acad. Sci. USA* **113** 6845–50

[16] Brandstetter M, Liertzer M, Deutsch C, Klang P, Schöberl J, Türeci H E, Strasser G, Unterrainer K and Rotter S 2014 *Nat. Commun.* **5** 4034
[17] Lin Z, Pick A, Lončar M and Rodriguez A W 2016 *Phys. Rev. Lett.* **117** 107402
[18] Wiersig J 2014 *Phys. Rev. Lett.* **112** 203901
[19] Wiersig J 2016 *Phys. Rev.* A **93** 033809
[20] Chen W, Özdemir Ş K, Zhao G, Wiersig J and Yang L 2017 *Nature* **548** 192
[21] Hodaei H, Hassan A U, Wittek S, Garcia-Gracia H, El-Ganainy R, Christodoulides D N and Khajavikhan M 2017 *Nature* **548** 187
[22] Vahala K J 2003 *Nature* **424** 839
[23] Cao H and Wiersig J 2015 *Rev. Mod. Phys.* **87** 61–111
[24] Wiersig J 2011 *Phys. Rev.* A **84** 063828
[25] Zhu J, Özdemir Ş K, He L and Yang L 2010 *Opt. Express* **18** 23535–43
[26] Lee S B, Yang J, Moon S, Lee S Y, Shim J B, Kim S W, Lee J H and An K 2009 *Phys. Rev. Lett.* **103** 134101
[27] Yi C H, Kullig J and Wiersig J 2018 *Phys. Rev. Lett.* **120** 093902
[28] Peng B, Özdemir Ş K, Rotter S, Yilmaz H, Liertzer M, Monifi F, Bender C M, Nori F and Yang L 2014 *Science* **346** 328–32
[29] Ge L and Stone A D 2014 *Phys. Rev.* X **4** 031011
[30] Shu F J, Zou C L, Zou X B and Yang L 2016 *Phys. Rev.* A **94** 013848
[31] Richter S, Michalsky T, Sturm C, Rosenow B, Grundmann M and Schmidt-Grund R 2017 *Phys. Rev.* A **95** 023836
[32] Heiss W D and Wunner G 2017 *Eur. Phys. J.* D **71** 312
[33] Demange G and Graefe E M 2012 *J. Phys. A: Math. Theor.* **45** 025303
[34] Jing H, Özdemir Ş K, Lü H and Nori F 2017 *Sci. Rep.* **7** 3386
[35] Zhong Q, Christodoulides D N, Khajavikhan M, Makris K G and El-Ganainy R 2018 *Phys. Rev.* A **97** 020105
[36] Schnabel J, Cartarius H, Main J, Wunner G and Heiss W D 2017 *Phys. Rev.* A **95** 053868
[37] Jebali A, Mahrt R F, Moll N, Erni D, Bauer C, Bona G L and Bächtold W 2004 *J. Appl. Phys.* **96** 3043–9
[38] Ochoa D, Houdré R, Ilegems M, Benisty H, Krauss T F and Smith C J M 2000 *Phys. Rev.* B **61** 4806–12
[39] Hentschel M and Richter K 2002 *Phys. Rev.* E **66** 056207
[40] Bäcker A, Ketzmerick R, Löck S, Wiersig J and Hentschel M 2009 *Phys. Rev.* A **79** 063804
[41] Ryu J W, Lee S Y and Kim S W 2012 *Phys. Rev.* A **85** 042101
[42] Schnabel J, Cartarius H, Main J, Wunner G and Heiss W D 2017 *Acta Polytech.* **57** 454–61
[43] Wilson K A, Finch C A, Anderson P, Vollmer F and Hickman J J 2015 *Biomaterials* **38** 86–96
[44] Foreman M R, Swaim J D and Vollmer F 2015 *Adv. Opt. Photon.* **7** 168–240
[45] Vollmer F and Yang L 2012 *Nanophoton* **1** 267
[46] Shao L, Jiang X F, Yu X C, Li B B, Clements W R, Vollmer F, Wang W, Xiao Y F and Gong Q 2013 *Adv. Mater.* **25** 5616–20
[47] Vollmer F, Arnold S and Keng D 2008 *Proc. Natl Acad. Sci. USA* **105** 20701–4
[48] Vollmer F and Arnold S 2008 *Nat. Methods* **5** 591
[49] He L, Özdemir S K, Zhu J, Kim W and Yang L 2011 *Nat. Nanotechnol.* **6** 428–32
[50] Zhu J, Özdemir S K, Xiao Y F, Li L, He L, Chen D R and Yang L 2010 *Nat. Photon.* **4** 46–9
[51] Schmidt-Grund R, Hilmer H, Hinkel A, Sturm C, Rheinländer B, Gottschalch V, Lange M, Zúñiga-Pérez J and Grundmann M 2010 *Phys. Status Solidi* b **247** 1351–64
[52] Benyoucef M, Shim J B, Wiersig J and Schmidt O G 2011 *Opt. Lett.* **36** 1317
[53] Bennett B R, Soref R A and Del Alamo J A 1990 *IEEE J. Quantum Electron.* **26** 113–22